A State-Dependent Quantification of Climate Sensitivity Based on Paleodata of the Last 2.1 Million Years

Peter Köhler[1] [iD], Lennert B. Stap[1,2] [iD], Anna S. von der Heydt[2] [iD], Bas de Boer[2] [iD], Roderik S. W. van de Wal[2] [iD], and J. Bloch-Johnson[3] [iD]

[1]Alfred-Wegener-Institut Helmholtz-Zentrum für Polar-und Meeresforschung (AWI), Bremerhaven, Germany, [2]Institute for Marine and Atmospheric research Utrecht (IMAU), Center for Extreme Matter and Emergent Phenomena, Utrecht University, Utrecht, Netherlands, [3]Department of the Geophysical Sciences, University of Chicago, Chicago, IL, USA

Abstract The evidence from both data and models indicates that specific equilibrium climate sensitivity $S_{[X]}$—the global annual mean surface temperature change (ΔT_g) as a response to a change in radiative forcing X ($\Delta R_{[X]}$)—is state dependent. Such a state dependency implies that the best fit in the scatterplot of ΔT_g versus $\Delta R_{[X]}$ is not a linear regression but can be some nonlinear or even nonsmooth function. While for the conventional linear case the slope (gradient) of the regression is correctly interpreted as the specific equilibrium climate sensitivity $S_{[X]}$, the interpretation is not straightforward in the nonlinear case. We here explain how such a state-dependent scatterplot needs to be interpreted and provide a theoretical understanding—or generalization—how to quantify $S_{[X]}$ in the nonlinear case. Finally, from data covering the last 2.1 Myr we show that—due to state dependency—the specific equilibrium climate sensitivity which considers radiative forcing of CO_2 and land ice sheet (LI) albedo, $S_{[CO_2,LI]}$, is larger during interglacial states than during glacial conditions by more than a factor 2.

1. Introduction

Global temperature rise due to the anthropogenic emissions of greenhouse gases will be a challenge for the years to come and are in the focus of climate research, also summarized in the International Panel on Climate Change (IPCC) assessment reports (Stocker et al., 2013). The expected change in equilibrium annual mean surface temperature due to a doubling of atmospheric CO_2 concentration is called equilibrium climate sensitivity (ECS), and when normalized by the given radiative forcing change caused by the expected anomaly in atmospheric CO_2 also named specific equilibrium climate sensitivity S. For a better quantification of S available climate simulations for the near future need to be compared and validated with whatever information is available for the paleoclimatic records (PALAEOSENS-Project Members, 2012).

One prominent approach (e.g., Köhler et al., 2015; Martínez-Botí et al., 2015; Rohling et al., 2012; von der Heydt et al., 2014) to calculate S (or following the nomenclature of PALAEOSENS-Project Members (2012), more precisely $S_{[X]}$) from paleodata is to evaluate the regression of scatterplots, in which global mean surface temperature anomaly (ΔT_g) has been plotted against radiative forcing anomalies ($\Delta R_{[X]}$), since following its definition,

$$S_{[X]} = \frac{\Delta T_g}{\Delta R_{[X]}}, \tag{1}$$

$S_{[X]}$ is easily obtained from the slope of a linear regression line, which needs to pass through the origin to avoid any biases. Passing through the origin ($\Delta T_g = 0$ K; $\Delta R_{[X]} = 0$ W m^{-2}) implies that no temperature change (with respect to a defined reference climate state) is detected for conditions without forcing anomalies. Usually, the preindustrial climate state serves as reference. Here X corresponds to the forcing processes considered, typically changes in CO_2 (sometimes also including the other greenhouse gases (GHG) CH_4 and N_2O), potentially corrected for some slow feedbacks such as planetary albedo changes caused by variations in land ice (LI), vegetation (VG) or dust (aerosols (AE)) (PALAEOSENS-Project Members, 2012). However, please note that in climate simulation studies used for the IPCC very often (but not always) $S_{[X]}$, as defined in equation (1), and what we here call "specific equilibrium climate sensitivity," is termed "climate sensitivity parameter." Once multiplied with the radiative forcing related to a doubling of atmospheric CO_2 concentration,

one might approximate or calculate Equilibrium Climate Sensitivity (ECS) or Earth System Sensitivity (ESS) (Lunt et al., 2010) out of $S_{[X]}$. In detail, from $S_{[CO_2]}$ one can calculate ESS, which represents the full reaction of the whole Earth System to a certain CO_2 radiative forcing. A paleodata-based ESS is comparable to results from Earth System Models with interactive ice sheets, vegetation, etc. Furthermore, from $S_{[CO_2,LI]}$ ECS can be approximated by considering land ice changes as a forcing in the paleodata (PALAEOSENS-Project Members, 2012). The such obtained ECS is comparable to results of climate models where land ice remains constant. An exact quantification of ECS, however, needs the consideration of corrections for all slow feedbacks (see equation (2) in PALAEOSENS-Project Members, 2012). $S_{[CO_2,LI]}$ is the most practical permutation of $S_{[X]}$, because the radiative forcing of many other slow processes are much more difficult to reconstruct.

In the review of the PALAEOSENS group in 2012 a quantitative expression of $S_{[X]}$ based on equation (1) was already included but only for individual data points, or whole time series. The state-dependent character of $S_{[X]}$ was already detected but could not be quantified in greater detail. Since then, climate sensitivity from paleodata has continued to be analyzed by regression analysis in the scatterplot of ΔT_g versus $\Delta R_{[X]}$ (e.g., Friedrich et al., 2016; Köhler et al., 2015; Martínez-Botí et al., 2015; von der Heydt et al., 2014).

The analysis of the problem is straightforward, if linear regression methods are applied, which implies that $S_{[X]}$ is a general property of the climate system. However, results point more and more in the direction that climate sensitivity is state dependent (e.g., Crucifix, 2006; Hargreaves et al., 2007; von der Heydt et al., 2016; Yoshimori et al., 2011), implying that for the $\Delta T_g - \Delta R_{[X]}$ scatterplot nonlinear regressions (e.g., higher-order polynomials) are describing the data more appropriate than a simple linear fit (Köhler et al., 2015; von der Heydt et al., 2014). In such cases the quantification of $S_{[X]}$ becomes more intricate and $S_{[X]}$ is not a general feature of the climate system anymore but state dependent. Note that some contribution to this nonlinearity might also be caused by the type of forcing with greenhouse gas forcing influencing the long-wave spectrum of the outgoing radiation having potentially a different effect than albedo changes influencing the amount of incoming short-wave radiation (e.g., Yoshimori et al., 2011).

The aim of this study is to investigate how we can quantify $S_{[X]}$ from a data set suggesting state-dependent behavior. We will further investigate climate records of the last 2.1 Myr, already discussed in Köhler et al. (2015). In the next section we will discuss the data that will be used for analysis. Section 3 will highlight some general insights on the system behavior from the scatterplots of ΔT_g versus $\Delta R_{[CO_2,LI]}$, while section 4 discusses different (practical) approaches how to calculate $S_{[CO_2,LI]}$ and quantify its state dependency. Note that while in section 3 we briefly discuss two specific aspects how the data analysis might influence the nonlinear characteristics found in the scattered data of ΔT_g versus $\Delta R_{[CO_2,LI]}$, the focus of this paper is not on the question whether we find such a nonlinearity (further discussion on that question are found in Köhler et al., 2015) but on how to quantify $S_{[X]}$, once you have detected its state-dependent character. This generalized view on the quantification of the state-dependent $S_{[X]}$ is new and a major step forward in extracting climate sensitivity from paleodata.

2. Data Over the Last 2.1 Myr

If we want to quantify $S_{[CO_2,LI]}$, time series of global annual mean surface temperature anomalies ΔT_g, radiative forcing of atmospheric CO_2 ($\Delta R_{[CO_2]}$) and land ice-based surface albedo forcing ($\Delta R_{[LI]}$) are necessary. Such time series have been compiled in Köhler et al. (2015) for the last 5 Myr. For such investigations how land ice-based surface albedo changes the radiative forcing $\Delta R_{[LI]}$ an energy balance model needs to be applied in order to calculate top of the atmosphere (or planetary albedo) changes, which are of relevance here. The energy balance model used here is described in Köhler et al. (2010). Here we investigate those data in more detail, focusing on the last 2.1 Myr, since the CO_2 data sets analyzed in Köhler et al. (2015), that reached beyond that point in time, led to results which are difficult to interpret. In particular, the best fits in scatterplots of ΔT_g against $\Delta R_{[CO_2,LI]}$ based on those data were far off the origin potentially indicating some systematic bias in the data. The climate variables used here (Figure 1) are based on the following (please refer to Köhler et al. (2015) for further details):

Global annual mean surface temperature change. An inverse approach was used to deconvolve the LR04 benthic $\delta^{18}O$ (Lisiecki & Raymo, 2005) into its sea level and temperature components (de Boer et al., 2014). This framework included 3-D ice sheet models and therefore also derived Northern Hemisphere (NH) temperature changes (ΔT_{NH}). Using information on the polar amplification factor (f_{pa}) from PMIP3/CMIP5 model output, the global annual mean surface temperature change was calculated after $\Delta T_g = \Delta T_{NH}/f_{pa}$.
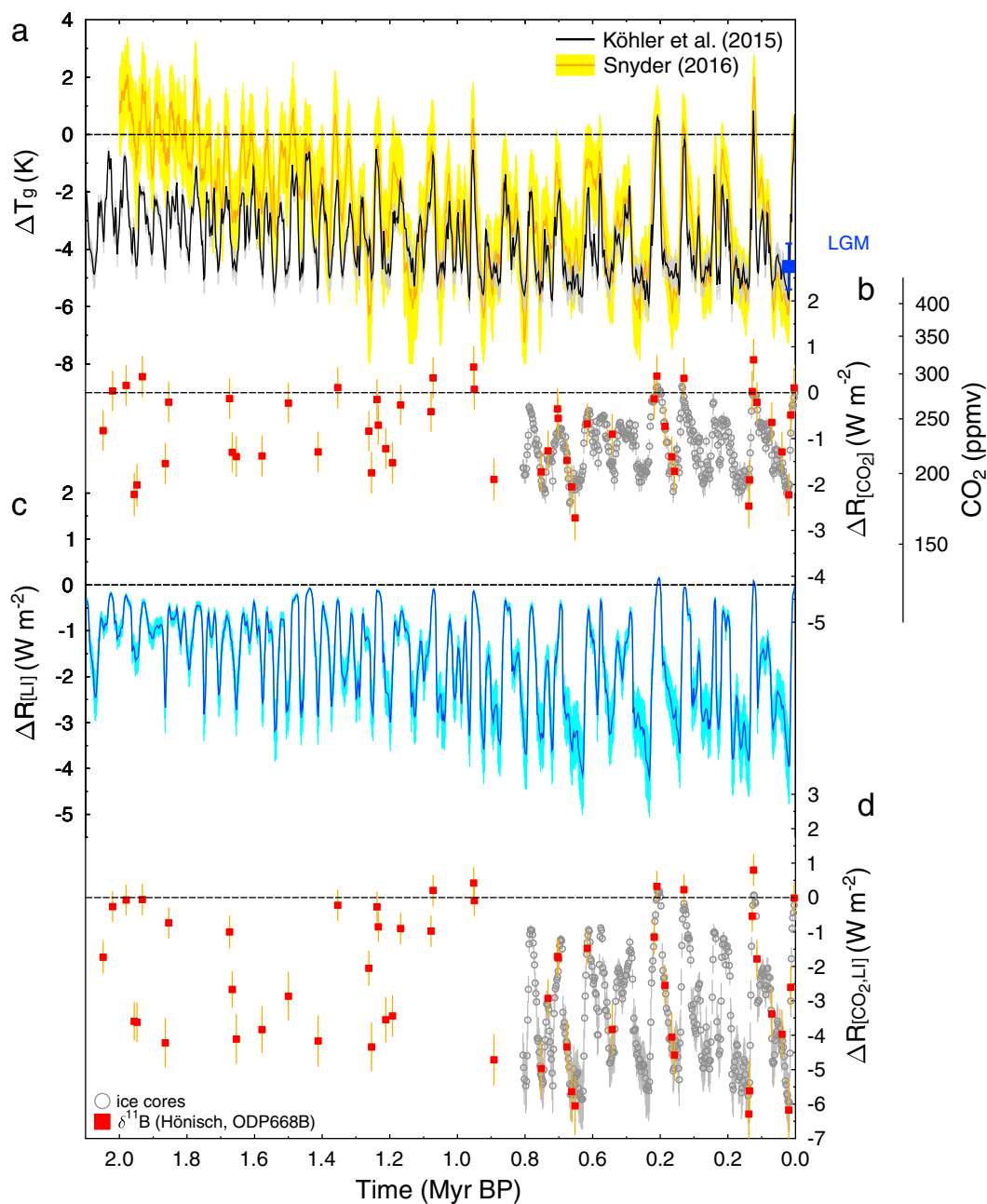
Figure 1. Changes in temperature and radiative forcing over the last 2.1 Myr. (a) Global mean surface temperature change ΔT_g. The approach of Köhler et al. (2015) used here and a more recent global temperature estimate of Snyder (2016) is plotted for comparison. Marked is the global cooling during the LGM derived from PMIP3/CMIP5 (blue square). (b) Changes in radiative forcing based on atmospheric CO_2 ($\Delta R_{[CO_2]}$). CO_2 data from ice cores (Bereiter et al., 2015) and based on $\delta^{11}B$ (Hönisch-lab, Hönisch et al., 2009). (c) Radiative forcing of land ice albedo $\Delta R_{[LI]}$. (d) The sum of the radiative forcing changes due to CO_2 and land ice sheets ($\Delta R_{[CO_2,LI]}$) whenever CO_2 data allow its calculation. Uncertainties show 1σ.

In Köhler et al. (2015) three different version of ΔT_g based on different assumptions on f_{pa} have been calculated. Here we use the standard version ΔT_{g1} that relates polar amplification linearly to northern hemispheric temperature. Note that conclusions in Köhler et al. (2015) did not depend on this choice in f_{pa}.

Radiative forcing from land ice. In the deconvolution approach of de Boer et al. (2014) the areal distribution of land ice area has also been simulated. This information together with the incoming solar insolation (Laskar et al., 2004) was used in a simplistic energy balance model (Köhler et al., 2010) to calculate in latitudinal

bands of 5° changes in radiative forcing $\Delta R_{[LI]}$. The novelty of this approach was that the combination of 3-D ice sheet models and their latitudinal dependency was leading to nonlinearities in the relationship between temperature change and radiative forcing change, which have so far been overlooked in other, more simplistic approaches (e.g., Hansen et al., 2013; Martínez-Botí et al., 2015; von der Heydt et al., 2014; van de Wal et al., 2011).

Radiative forcing from CO_2. Ice core-based CO_2 data cover the last 800 kyr. They have been stacked in Bereiter et al. (2015) but are based on various different ice cores (EPICA Dome C, EPICA Dronning Maud Land, Law Dome, Siple Dome, Talos Dome, Vostok, West Antarctic Ice Sheet Divide) and studies (Ahn & Brook, 2014; Bereiter et al., 2012, 2015; MacFarling-Meure et al., 2006; Marcott et al., 2014; Monnin et al., 2001, 2004; Petit et al., 1999; Rubino et al., 2013; Schneider et al., 2013; Siegenthaler et al., 2005). Additionally, CO_2 based on $\delta^{11}B$ isotopes ($n = 52$ data points) from the Hönisch-lab have been published (Hönisch et al., 2009), which cover the last 2.1 Myr and agree with the ice core data during their overlap. The radiative forcing of CO_2 is calculated after $\Delta R_{[CO_2]} = 5.35 \cdot \ln(CO_2/278 \text{ ppm})$ W m^{-2} (Myhre et al., 1998).

ΔT_g and $\Delta R_{[LI]}$ are available at time intervals of 2 kyr. Therefore, all ice core CO_2 data have been resampled to the same temporal spacing, and CO_2 from the Hönisch-lab have been aligned to the nearest simulation output. Only time steps, for which all three relevant records exist are used for further analysis. Since both ΔT_g and $\Delta R_{[LI]}$ are based on a model-based interpretation of the LR04 benthic $\delta^{18}O$ stack (Lisiecki & Raymo, 2005), which itself has temporal resolutions of 2 ka and above for data older than 600 kyr and of 1 kyr for younger samples only little impact is expected from the 2 kyr resampling of the time series.

A more recent global temperature stack (Snyder, 2016) agrees with our approach within the uncertainties for the last 1.2 Myr. Temperature reconstructions differ further back in time with higher temperatures found in the stack of Snyder (2016), which is based on sea surface temperature reconstructions only. We therefore conclude that the analysis of the data based on ice core CO_2 covering the last 800 kyr is in agreement with this new temperature stack while that based on the Hönisch CO_2 data might need further refinements. We here refrain from using the new temperature change record of Snyder (2016) since in our approach ΔT_g and $\Delta R_{[LI]}$ are closely related to each other. In future studies a new calculation of land ice distribution might be performed that considers the temperature information of Snyder (2016), but this is beyond the scope of this study.

3. General Insights From $\Delta T_g - \Delta R_{[CO_2,LI]}$ Scatterplots

In the previous study we have used polynomial fits to the data to discriminate between a linear or nonlinear relationship in $\Delta T_g - \Delta R_{[CO_2,LI]}$ scatterplots (Köhler et al., 2015). Those data sets based on CO_2 data from ice cores or the Hönisch-lab, initially analyzed in Köhler et al. (2015), revealed that a higher-order polynomial best fit the scattered $\Delta T_g - \Delta R_{[CO_2,LI]}$ data indicating a state dependency in $S_{[CO_2,LI]}$. While in this initial study we first investigated the relationship between both variables more general, for example, allowing the fits to disagree with the origin, we here have our focus on the quantification of $S_{[CO_2,LI]}$ and therefore demand as additional constraint that $\Delta T_g = 0$ K for $\Delta R_{[CO_2,LI]} = 0$ W m^{-2}. Furthermore, we expand on these previous analyses by investigating two additional questions:

How important is the decision which variable is plotted on the x axis for the detection of this nonlinearity/state dependency? While most previous studies perform a regression with $\Delta R_{[X]}$ on the x axis (treating ΔT_g as the dependent and $\Delta R_{[X]}$ as the independent variable), there are arguments to be made for also trying a regression with the axes flipped (i.e., ΔT_g on the x axis). In particular, if the fast and slow feedbacks that determine the climate sensitivity depend in a linear (or polynomial) way on the temperature, this would lead to $\Delta R_{[X]}$ being a polynomial function of ΔT_g, and not vice versa. Also, if there was a bifurcation in the Earth's climate — such as occurred during the Snowball Earth, or, potentially, to a hothouse climate (e.g., Pierrehumbert et al., 2011) — a regression with $\Delta R_{[X]}$ on the x axis would not capture the bifurcation, since there would be multiple ΔT_g's for the same $\Delta R_{[X]}$, while a regression with ΔT_g on the x axis would capture this bifurcation, as there would still be only one $\Delta R_{[X]}$ for each ΔT_g. For these reasons, it seems worth exploring if the choice of independent variable changes our analysis.

Note that scatterplots of $\Delta R_{[X]}$ against ΔT_g are different than the plots of net top-of-atmosphere flux against surface temperature commonly found in studies of climate simulations subjected to abrupt forcing, often known as "Gregory plots" (Gregory et al., 2004). These studies analyze how simulations relax back to their

Table 1
Fitting a Linear or a Nonlinear Function to the Data With the Precondition to Meet the Origin ($a = 0$)

			χ^2			1st versus 2nd		2nd versus 3rd				r^2
Data set	x axis	n	1st	2nd	3rd	F	p	F	p	m	L	%
Ice cores	$\Delta R_{[CO_2,LI]}$	394	3,027	1,334	1,200	497.5	<0.001	46.9	<0.001	3rd	**	71
Ice cores	ΔT_g	394	1,944	1,882	1,837	12.9	<0.001	9.6	<0.01	3rd	*	63
Hönisch	$\Delta R_{[CO_2,LI]}$	52	661	441	427	24.9	<0.001	1.6	0.21	2nd	**	65
Hönisch	ΔT_g	52	192	169	162	6.8	0.01	2.1	0.15	2nd	*	74

Note. The 5,000 Monte Carlo-generated realizations of the scattered $\Delta T_g - \Delta R_{[CO_2,LI]}$ were analyzed. The data are randomly picked from the entire Gaussian distribution described by the 1σ of the given uncertainties in both ΔT_g and $\Delta R_{[CO_2,LI]}$. The parameter values of fitted polynomials are given as mean $\pm 1\sigma$ uncertainty from the different Monte Carlo realizations using as ΔT_g the ΔT_{g1} calculated in Köhler et al. (2015). Data sets differ in the underlying CO_2 data (ice cores (800 kyr) or Hönisch-lab (2.1 Myr)). Analyses differ by which variable is assumed to be the independent variable to be plotted on the x axis ($\Delta R_{[CO_2,LI]}$ or ΔT_g). n: number of data points in data set; χ^2: weighted sum of squares following either first-, second-, or third-order polynomials; F: F ratio for F test to determine if the higher-order fit describes the data better than the lower order fit (first-versus second-order polynomial or second- versus third-order polynomial); p: p value of the F test; m: order of significant polynomial; L: significance level of F test (*: significant at 1 % level ($0.001 < p \leq 0.01$); **: significant at 0.1 % level ($p \leq 0.001$)); r^2: correlation coefficient of the fit.
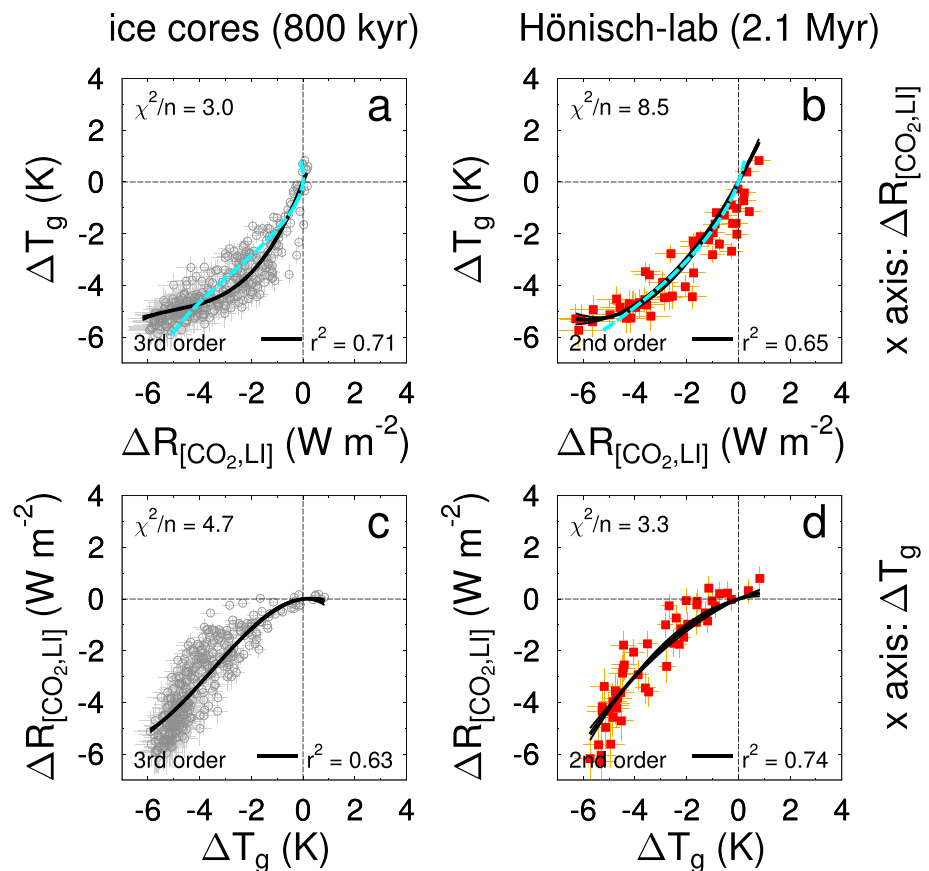

Figure 2. Scatterplots of data of global temperature change ΔT_g against radiative forcing $\Delta R_{[CO_2,LI]}$. ΔT_g is calculated with the polar amplification factor f_{pa} being a linear function of ΔT_{NH}. Radiative forcing of CO_2 together with land ice (LI) albedo with CO_2 based on (left, gray points) ice cores (Bereiter et al., 2015) or (right, red points) $\delta^{11}B$ from Hönisch-lab (Hönisch et al., 2009). (a and b) Radiative forcing plotted on x axis. (c and d) ΔT_g plotted on x axis. Black lines show average best fits (second- or third-order polynomials) to 5,000 Monte Carlo realizations of the data (details in Table 1). Cyan broken lines in Figures 2a and 2b show additionally the regressions obtained in Figures 2c and 2d with flipped axes to facilitate comparisons. Each subfigure contains the mean uncertainty of the fit by dividing χ^2 (the weighted sum of squares from the regression analysis) by n and the correlation coefficient r^2. Uncertainties show 1σ.
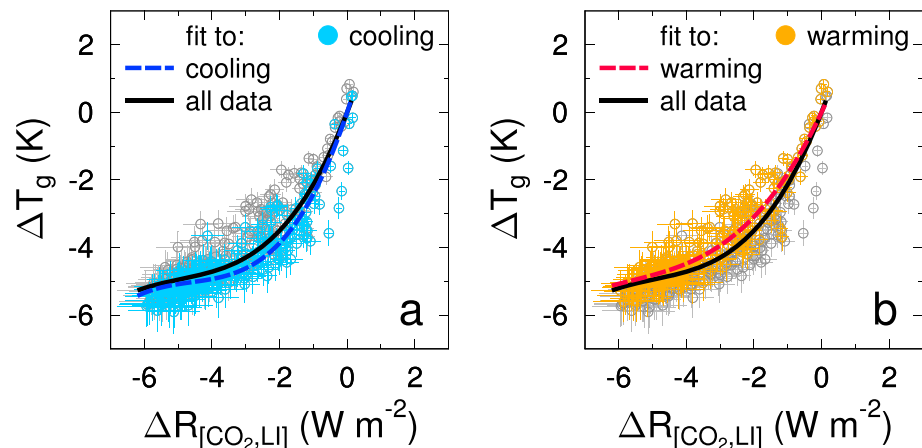
Figure 3. Scatterplots of ice core-based data of global temperature change ΔT_g against radiative forcing $\Delta R_{[CO_2,LI]}$, which distinguish between (a) cooling ($\delta(\Delta T_g)/\delta t < 0$) and (b) warming ($\delta(\Delta T_g)/\delta t \geq 0$). Lines are Monte Carlo-based averages ($n = 5,000$) of third-order polynomial through the origin, black for all data.

attractor after being perturbed away from it, and therefore, their trajectories need not reflect the relationship between radiative forcing and equilibrium warming (Armour et al., 2013). While one of the authors used climate simulations to trace this relationship in a previous study (Bloch-Johnson et al., 2015), generating plots of ΔT_g versus $\Delta R_{[X]}$, the resulting curve does not account for the slow feedbacks that one would expect to find in the paleoclimate record and so is likely different than what would be found in paleodata (von der Heydt & Ashwin, 2016). As a result, while studies of climate simulations sometimes find state dependence (Bloch-Johnson et al., 2015; Jonko et al., 2013; Meraner et al., 2013), it is a separate question to investigate from paleodata if $S_{[X]}$ is state dependent.

When exchanging axes for both data sets (CO_2 from ice cores for the last 800 kyr and based on Hönisch-lab reconstruction for the last 2.1 Myr) and applying the same rigorous statistics as before (Monte Carlo approach to consider uncertainties in both directions, 5,000 replicates, F test statistics to establish if higher-order polynomials better fit the data), we find similar nonlinearities (Table 1 and Figure 2) indicating that the choice of the axes is negligible. Note that we restrict all analyses to cases, in which the fits meet the origin. While nonlinear regression lines for the Hönisch-lab data with the different choices of the axes also agree reasonable well when plotted again in the same plot (see Figure 2b), regression lines for the ice core data diverge for glacial conditions (see Figure 2a). This divergence might be caused by the third-order polynomial fitted to the ice core data (while at best a second-order polynomial was fitted to the Hönisch-lab data). It shows that while the nonlinearity between $\Delta R_{[CO_2,LI]}$ and ΔT_g does not depend on the choice of the axes, the simplified quantification of the relationship between both variables is in detail depending on this choice.

Is there a different relationship for those data, which describe global cooling or a glaciation versus those that describe global warming or a deglaciation? For the data set based on the ice core CO_2 this information can be gained when comparing each data point with its precursor, finally calculating $\delta(\Delta T_g)/\delta t$. For the Hönisch-lab-based CO_2 data the distance between neighboring data points is too large to come to a meaningful results here. Ice core-based CO_2 data are nearly equally distributed into warming (49%) and cooling (51%) periods. Using the same Monte Carlo approach as before with 5,000 replicates and taken data uncertainty in both directions into account, we found a higher nonlinearity (stronger bend of the higher-order polynomial fitting the data) in those data obtained from cooling climatic conditions (Figure 3). This is in agreement with a recent analysis of paleodata, in which a pronounced decoupling of the orbital (7 kyr running mean) components of atmospheric CO_2 and temperature during phases of decreasing obliquity has been detected (Hasenclever et al., 2017). During declining obliquity land ice sheets are build up synchronous to long-term cooling (glaciation). Atmospheric CO_2 levels, which during obliquity rise closely follow the observed global warming, are during obliquity fall decoupled from temperature change, that is, decreases on the order of 10 kyr later. This decoupling is possibly caused by CO_2 outgassing from mid-ocean ridge and hot spot volcanism triggered by falling sea level.

The new insights from these two questions are fundamental, since they (i) support the natural choice of the axes used in paleoclimate (data based) research and (ii) highlight again that a dominant part of the nonlinearity in the climate system (and therefore the state dependency in $S_{[X]}$) is connected to land ice sheet growth.

Furthermore, to the naked eye, it seems that the nonlinear regressions heavily depends on the few data points obtained from interglacial conditions, for example, close to the origin. One might therefore be interested if the detected nonlinearity changes (or potentially vanishes and again a linear relationship is found) once these points are slightly shifted or neglected in the regression analysis. Our nonlinear regression analysis only weakly depends on them, since all regressions are forced to meet the origin in order to find no temperature change for no forcing change. For further details on the nonlinearity please refer to our preceding study (Köhler et al., 2015).

4. Quantifying the State Dependency of $S_{[X]}$

In the previous section we have discussed how to detect state dependency from the scatterplots of ΔT_g and $\Delta R_{[CO_2, LI]}$ data, but we have not yet quantified $S_{[CO_2, LI]}$ for the different climate states or regimes. This quantification depends on the way the data are analyzed, as we will discuss below. The different approaches will be first applied to the ice core data of the last 800 kyr. We finally quantify $S_{[CO_2, LI]}$ also from data of the last 2.1 Myr based on CO_2 proxy data from the Hönisch-lab.

We assume that the information obtained from the paleodata refers to quasi-equilibrium climates, implying that atmosphere and ocean are equilibrated, but not the ice sheets, also not containing the full response of atmosphere and ocean to the changing ice sheets. This might be a simplification, since in climate simulations it takes on the order of a few thousand years after an imbalance in Earth's energy budget until a new equilibrium surface temperature has been established (e.g., Hansen et al., 2011), and including ice sheet will lead to an even much longer equilibrium time scale. The quasi-equilibrium assumption taken here should nevertheless be valid. It has been tested in similar data sets (see supporting information in PALAEOSENS-Project Members, 2012). Furthermore, abrupt climate changes connected with Dansgaard-Oeschger or similar events are not contained in the output of the 3-D ice sheet models (de Boer et al., 2014), from which we calculate global temperature change ΔT_g and land ice albedo radiative forcing $\Delta R_{[LI]}$. How a time-dependent climate sensitivity might be calculated is not within the scope of this study but was investigated elsewhere (e.g., Rohling et al., 2018; von der Heydt & Ashwin, 2016; Zeebe, 2013).

The easiest and most robust estimate of $S_{[CO_2, LI]}$ is obtained, when $S_{[CO_2, LI]}$ is calculated individually for each time step t_i out of $\Delta T_g(t_i)$ and $\Delta R_{[CO_2, LI]}(t_i)$ (Figure 4d). Taking the uncertainties of the individual data points into account, a probability density functions (PDF) of $S_{[CO_2, LI]}$ is calculated straightforward (Figure 4f), from which the median, the most likely, and the spread (uncertainty distribution) within $S_{[CO_2, LI]}$ can be obtained. If the underlying data set of the PDF is split into various subsets (here distinguishing data for two different radiative forcing domains, Figure 4e) a first, rough quantification of the state dependency of $S_{[CO_2, LI]}$ is generated and has already been obtained in Köhler et al. (2015). One known problem of this approach is that for small disturbances in the radiative forcing ($\Delta R_{[CO_2, LI]}$ close to zero) one might obtain in the point-wise calculations of $S_{[CO_2, LI]}$ unrealistically high and low values. Such values might be caused by dating uncertainties of the underlying paleorecords or transient effects (de Boer et al., 2012). In our analysis in Köhler et al. (2015) we found 20 outliers (from 394 data points contained in Figure 4) that did not match in the realistic range of $S_{[CO_2, LI]}$ between 0 and 3 K W^{-1} m^2, and they have been rejected from further analysis. Furthermore, from those data with $\Delta R_{[CO_2, LI]}$ close to zero, which have not been rejected, calculated values of $S_{[CO_2, LI]}$ seemed to follow a different pattern than the rest of the data (Figure 4e). Again, we understand these anomalies to be probably based on dating uncertainties, nonnegligible influence of transient climate response, and the problem that the ratio from two small numbers might easily contain a large error.

4.1. Approach I: The Point-Wise Approach

A state-dependent equation of the specific equilibrium climate sensitivity $S_{[X]}$ might be obtained from analyzing the paleodata in greater detail. To do so, a function has to be found that relates the temperature perturbations ΔT_g to radiation perturbations $\Delta R_{[X]}$. It is not necessary that such a function is developed analytically; it can be derived from nonlinear regression analysis of the scattered data. For reasons of simplicity
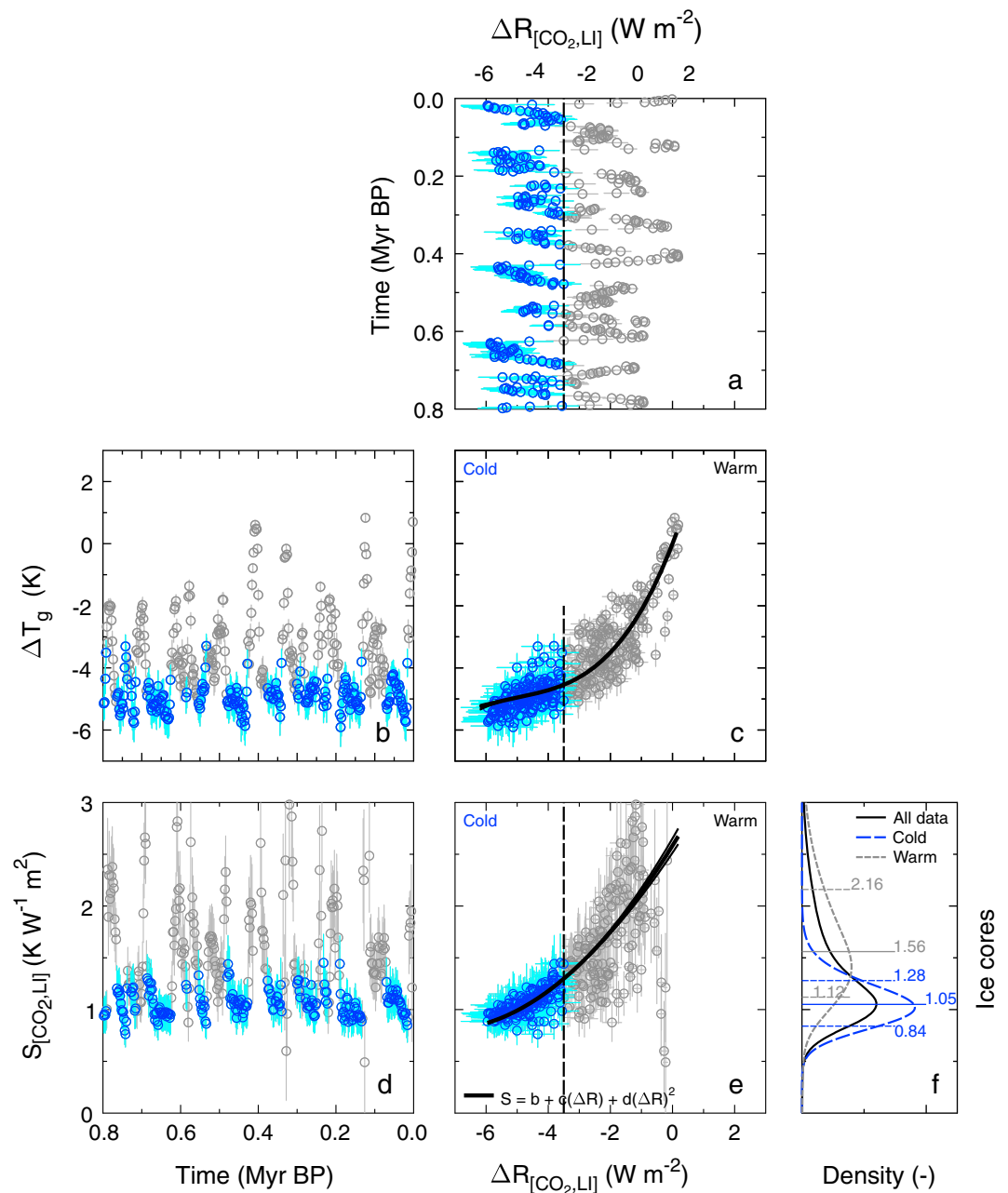
Figure 4. Data of the last 0.8 Myr analyzed for specific equilibrium climate sensitivity $S_{[CO_2,LI]}$. In all subplots data are split into data from "warm" (gray) and "cold" (blue) periods distinguished by $\Delta R_{[CO_2,LI]} = -3.5$ W m^{-2}. (a) Time series of radiative forcing $\Delta R_{[CO_2,LI]}$ caused by CO_2 (Bereiter et al., 2015), corrected by land ice albedo feedback (de Boer et al., 2014; Köhler et al., 2015). (b) Time series of global surface temperature change ΔT_g (Köhler et al., 2015). (c) Scatterplot of ΔT_g versus $\Delta R_{[CO_2,LI]}$ including a best fit through the origin. (d) Time series of point-wise calculated specific equilibrium climate sensitivity $S_{[CO_2,LI]}$. Only data with their mean in $S_{[CO_2,LI]}$ in the range [0, 3] K W^{-1} m^2 are analyzed and plotted. (e) Same data as in Figure 4d in a scatterplot of $S_{[CO_2,LI]}$ against radiative forcing $\Delta R_{[CO_2,LI]}$. Thick line is the calculated state-dependent $S_{[CO_2,LI]}(\Delta R_{[CO_2,LI]})$ derived from the third-order nonlinear fit through the $\Delta T_g - \Delta R_{[CO_2,LI]}$ data with the additional condition to meet the origin ($a = 0$). (f) Probability density distribution of ice core-based $S_{[CO_2,LI]}$. (f) Labels denote 16th, 50th, and 84th percentile.
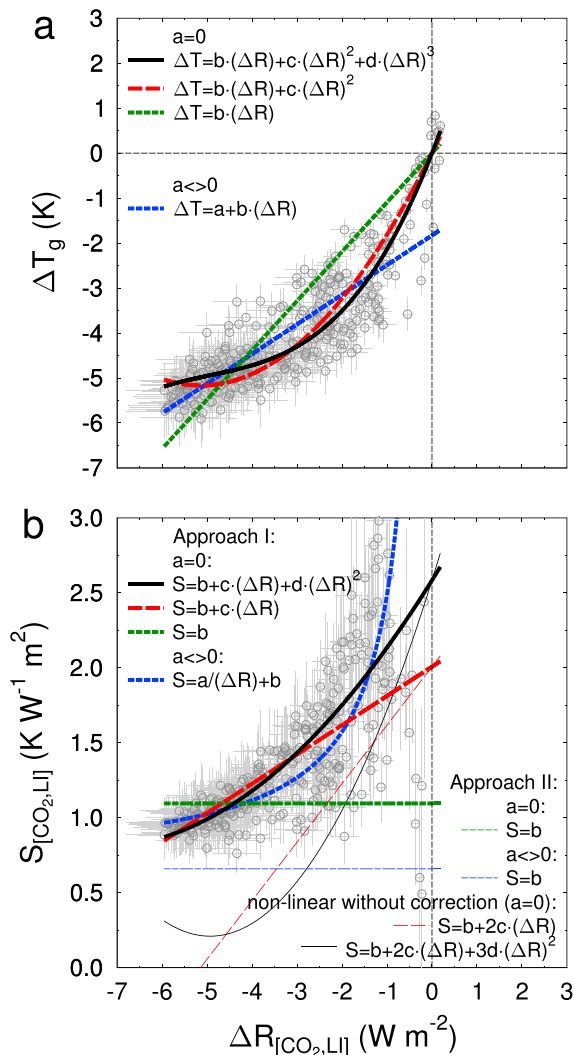
Figure 5. Illustrating of the differences in the calculation of $S_{[CO_2,LI]}$ when based either on approach I (quantification of point-wise results, S^{pw}) or on approach II (linear slope, S^{slope}) for different orders of the polynomial fit to the data. (a) Scatterplot of ΔT_g versus $\Delta R_{[CO_2,LI]}$ including various different fits to the data. We compare two different linear fits (best fit (blue, $\Delta T = -1.83 + 0.66 \cdot (\Delta R)$) or with the additional constrain to pass through the origin ($a = 0$, green, $\Delta T = 1.10 \cdot (\Delta R)$) with second- (red, $\Delta T = 2.01 \cdot (\Delta R) + 0.20 \cdot (\Delta R)^2$) and third- (black, $\Delta T = 2.58 \cdot (\Delta R) + 0.48 \cdot (\Delta R)^2 + 0.03 \cdot (\Delta R)^3$) order polynomial. From Monte Carlo statistics and F tests the third-order fit was chosen to fit the data best (Köhler et al., 2015). (b) Scatterplot of the corresponding $S_{[CO_2,LI]}$ versus $\Delta R_{[CO_2,LI]}$ data including the different fits to the data for both approaches I (S^{pw}, equation (3) and the uncorrected approach II (S^{local}, equation (5). Results of approach II agree with results of approach I when they are corrected following equation (11). The results for $S_{[CO_2,LI]}$ based on the linear fit to the data with $a = 0$ are identical for both approaches (green line), therefore not distinguishable. Detailed functions in Figure 5b are easily derived from the given equations for fits in Figure 5a. Uncertainties in the parameter values are omitted for clarity.

both variables are described in the following by ΔT and ΔR. For nonlinear description of ΔT as a function of ΔR a higher-order polynomial is the most obvious choice (but other equations are possible):

$$\Delta T(= f(\Delta R)) = a + b\Delta R + c\Delta R^2 + d\Delta R^3 + \dots \quad (2)$$

Climate sensitivity can then be calculated as

$$S^{pw} = \frac{\Delta T}{\Delta R} = \frac{a}{\Delta R} + b + c\Delta R + d\Delta R^2 + \dots \quad (3)$$

This approach is called *point-wise* (pw) since the derived equation in the $S-\Delta R$ data space agrees with the individual data points (Figures 4e and 5b). Please note that in all plots of S against ΔR (Figures 4e, 5b, and 6a) the plotted regressions are not based on any analysis of the relationship between these two variables (which are due to the dependency of S against ΔR statistically not robust) but on the analysis of the underlying $\Delta T-\Delta R$ plots. The reference climate has to be chosen such that $a = 0$, to ensure finite climate sensitivity at $\Delta R = 0$. In the above case, climate sensitivity is constant (i.e., not state dependent) if the higher-order terms are zero: $c = d = 0$. Otherwise, climate sensitivity is a function of the radiation perturbation and therefore state dependent. This approach has been applied for the ice core data and is contained in Figure 4e.

Please also note the following: When calculating PDFs based on single points (e.g., as done in Köhler et al., 2015) each data point is weighted with equal weight. This is different from approaches in which regression functions are applied. For example, in linear regressions which would be applied for the state-independent case, the frequently applied regression method of ordinary least squares (OLS) minimizes the sum of squared residuals, which leads to a higher weight for data points farther away from the origin.

4.2. Approach II: Using Local Slopes (Piece-Wise Linear Analysis)

In the constant case ($c = d = 0$), climate sensitivity can also be found by taking the *local slope* of the T-R-relation, therefore called S^{local}:

$$S^{local} = \frac{\delta \Delta T}{\delta \Delta R} = b. \quad (4)$$

However, in the state-dependent case

$$S^{local} = \frac{\delta \Delta T}{\delta \Delta R} = b + 2c\Delta R + 3d\Delta R^2 + \dots \quad (5)$$

Now S^{local} (equation (5)) is evidently not equal to the point-wise-calculated climate sensitivity S^{pw} (equation (3)). For illustrative purposes we have included some realization of S based on local slopes in Figure 5b. Clearly, they disagree from results obtained with the point-wise approach. Indeed, the suggested equations do not meet the scattered data of $S_{[CO_2,LI]}$ versus $\Delta R_{[CO_2,LI]}$.

The condition for state dependency, however, remains the same: The higher-order terms have to be nonzero. For the local slope case, this means that the slope is nonconstant.

4.3. Combining Data-Based Approaches and Model Results

Climate models usually perturb a reference climate $\{R_0; T_0\}$, and end up with a new climate $\{R_1; T_1\}$. They consider climate sensitivity in the following way:

$$S^{model} = \frac{T_1 - T_0}{R_1 - R_0}. \quad (6)$$

One might argue that only radiative forcing anomalies are of interest, and not the absolute radiative forcings R_0 and R_1, so the denominator in equation (6) should be ΔR_1. For the sake of generalization we keep equation (6) as is, but the reader will see below (equation (9)) how relevant this formulation might be.
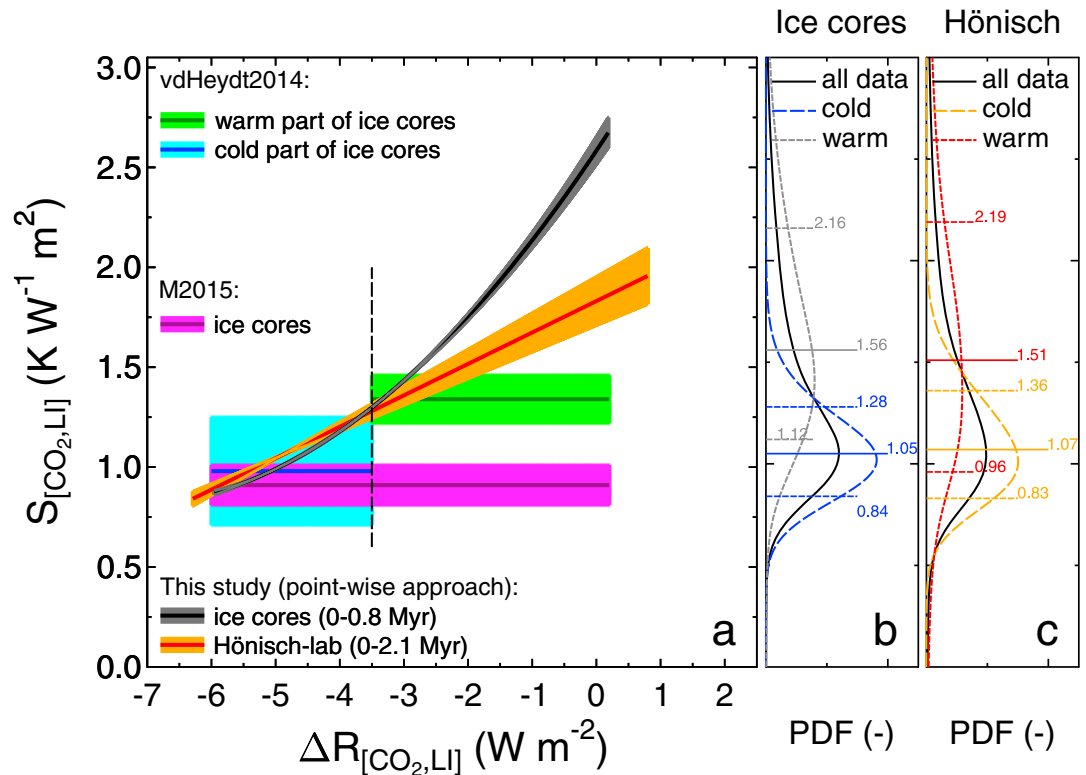
Figure 6. Revised calculation of $S_{[CO_2,LI]}$ (a) following the quantification of the point-wise approach I (S^{pw}, this study). Results based on the ice core data of the last 0.8 Myr and based on the Hönisch data over the last 2.1 Myr (Hönisch et al., 2009) are compared with previous estimates of von der Heydt et al. (2014) (vdHeydt2014) and of Martínez-Botí et al. (2015) (M2015). (b and c) PDFs based on the same data, as already contained in Köhler et al. (2015), are plotted, including the 16th, 50th, and 84th percentile in the "warm" and "cold" data regimes. Vertical broken line in Figure 6a marks where the PDFs in Figures 6b and 6c distinguish "cold" from "warm" data.

Equation (2), the higher-order polynomial fit of temperature versus forcing, is also valid, if based on absolute values in T and R, so one might fit in a model-output T versus R scatterplot:

$$T(= f(R)) = a + bR + cR^2 + dR^3 + \dots \tag{7}$$

Using this approach would imply (using equation (7), here reduced for simplicity to a second-order polynomial)

$$S^{model} = \frac{b(R_1 - R_0) + c\left(R_1^2 - R_0^2\right)}{R_1 - R_0}. \tag{8}$$

Now, if the reference climate $\{R_0; T_0\}$ happens to be the preindustrial reference climate (which is not always the case), we have $\Delta R_1 = R_1 - R_0$; $\Delta T_1 = T_1 - T_0$, then

$$S^{model} = \frac{b\Delta R_1 + c\Delta R_1^2 + 2cR_0\Delta R_1}{\Delta R_1} = (b + 2cR_0) + c\Delta R_1 = b' + c\Delta R_1, \tag{9}$$

with $b' = (b + 2cR_0)$. Equation (9) is equal to approach I, the point-wise quantification of climate sensitivity (S^{pw}), but the parameter b' of the nonlinear regression is depending on the reference climate, in detail the radiative forcing R_0.

More generally, S can be obtained from S^{local}, by the following equation:

$$S = \frac{1}{R_2 - R_1} \int_{R_1}^{R_2} S^{local} \, d\Delta R. \tag{10}$$

$$= \frac{1}{\Delta R_2 - \Delta R_1} \int_{\Delta R_1}^{\Delta R_2} S^{local} \, d\Delta R, \tag{11}$$

with $\Delta R_i = R_i - R_0$, where R_i stands for either R_1 or R_2. Equation (11) is generally valid for both model and data-based approaches and one central finding of our study and agrees in case of the reference climate being the preindustrial periods with S^{pw} (approach I). In other words, point-wise climate sensitivity is a measure of the mean local slope climate sensitivity over the radiation perturbation interval.

5. Discussions, Conclusions, and Implications

Following these different approaches explained above and its applications to the data sets investigated in Köhler et al. (2015), we find the following:

In case no state dependency in $S_{[X]}$ is found the data in the $\Delta T_g - \Delta R_{[X]}$ can be analyzed by linear regressions to derive the slope that is after $S_{[X]} = \frac{\Delta T_g}{\Delta R_{[X]}}$ an estimate of $S_{[X]}$. Be aware that approaches that combine point-wise-derived values of $S_{[X]}$ in a probability density function to a more general number treat all individual data points with the same weight, while data far away from the origin get a higher weight in linear regression analysis using OLS.

If state dependency of (specific) equilibrium climate sensitivity is found one has to be careful when quantifying equilibrium climate sensitivity $S_{[X]}$. The results based on local slopes are not directly comparable to estimates based on models or point-wise calculations; they can however be transferred into each other: The results based on local slopes transfer in results based on models or on the point-wise analysis by calculating the integral over the radiation perturbation interval following equation (11), which is one main finding of our study.

The local slope and point-wise approaches are not the same, in particular, when the function is strongly nonlinear, because the point-wise approach constructs lines between different points on a function independent of how far they are separated. The local slope approach instead constructs tangents along the function and does not need a reference point. As long as one analyses a regime of data where there exists a reasonable functional dependence between $\Delta R_{[X]}$ and ΔT_g, the point-wise approach is probably more practical. But if there is a regime shift hidden in the data, which we (by uncertainties) overlook and interpret as strongly nonlinear polynomial, then the point-wise approach gives incorrect estimates of $S_{[X]}$.

Taken at face value, the more sophisticated quantification of $S_{[CO_2,LI]}$ as a function of radiative forcing perturbation $\Delta R_{[CO_2,LI]}$ obtained here from the data sets described in Köhler et al. (2015) leads to numbers, which are by a factor of about 2 to 2.7 higher during climate conditions representing interglacials of the Pleistocene (last 2.1 Myr) than during full glacials during this period (Figure 6). The higher number for warmer climates are qualitatively also supported by a recent study, in which output from 785 kyr of climate simulations have been analyzed in a similar manner (Friedrich et al., 2016), although in that study $S_{[GHG,LI,AE]}$ and $S_{[GHG,LI,AE,VG]}$ have been quantified.

A previous approach based on first-order local slopes (von der Heydt et al., 2014) already suggested higher $S_{[CO_2,LI]}$ during interglacials than during glacials for data of the last 800 kyr, though only by 40%, while other approaches (Martínez-Botí et al., 2015) did not consider state dependency within the data set covering the last 800 kyr. These previous results agree more with the results we obtain for full glacial conditions. This might be the case, because linear regressions might not be forced through the origin. When comparing results based on PDFs with the other approaches (as done in Figure 9 in Köhler et al. (2015)) the difference might also be explained because in linear regressions data points farther away from the origin get a higher weight. The reason of this cold bias is not necessarily caused by the fact that most data are available for cold climates, as data may be binned, which has been tested in von der Heydt et al. (2014) and Köhler et al. (2015).

Interglacial climate conditions ($\Delta R_{[CO_2,LI]} \sim 0$ W m^{-2}, Figure 6) have a specific equilibrium climate sensitivity $S_{[CO_2,LI]}$ between 2.0 K W^{-1} m^2 (data of the last 2.1 Myr based on Hönisch-lab CO_2-proxies) and 2.7 K W^{-1} m^2 (ice core CO_2 data of the last 800 kyr). However, since both data sets investigated here mainly sample colder than present climates, these quantifications of $S_{[CO_2,LI]}$ during interglacials are situated at the higher end of the covered data range and might be taken with caution. They are clearly at the upper end of ranges of $S_{[CO_2,LI]}$ reported so far from various data sets of the last 65 Myr, for example, in PALAEOSENS-Project Members (2012), Figure 3, the 95% probability in $S_{[CO_2,LI]}$ ranged from 0.48 to 1.91 K W^{-1} m^2. Transferring these results based on data of the last Pleistocene to the near future remains difficult, since these paleodata cover mainly conditions with negative radiative forcing anomaly, while for the future positive radiative forcing anomalies related

to a rise in CO_2 are of interest, which obstructs a comparison as we showed that $S_{[CO_2,LI]}$ depends on $\Delta R_{[CO_2,LI]}$. Furthermore, $S_{[CO_2,LI]}$ needs to be corrected by factors related to fast and slow feedbacks to derive S^a, the actual or Charney climate sensitivity, which is via the multiplication with the radiative forcing of a CO_2 doubling ($\Delta R_{2\times CO_2} = 3.7$ W m^{-2}) directly related to corresponding warming, $\Delta T_{2\times CO_2}$, that is also constrained with climate models (see equation (2) in PALAEOSENS-Project Members, 2012). Corrections for not considered slow processes, including one for land ice sheet albedo which we included here, would have been necessary (but has not been considered) in Snyder (2016) who estimated $\Delta T_{2\times CO_2}$ based solely on the GHG forcing during the period 100–700 kyr BP. Snyder (2016) found the median of $S_{[GHG]}$ to vary between 1.8 and 2.8 K W^{-1} m^2 and, including the uncertainties, translated these values into a 95% confidence interval of $\Delta T_{2\times CO_2}$ of 7–13 K. The ommision of the necessary corrections of $S_{[GHG]}$ led to values in $\Delta T_{2\times CO_2}$ which are significantly higher than in other approaches, while the values of the underlying $S_{[GHG]}$ agreed with values found by others, for example, in PALAEOSENS-Project Members (2012) $S_{[GHG]}$ of 2.32 ± 0.76 (1σ) K W^{-1} m^2 of the last 800 kyr has been found. This overestimation of global warming in Snyder (2016) has already been discussed in Schmidt et al. (2017) and highlights that like-with-like comparisons, for example, with $S_{[X]}$ found in other studies, are probably a robust approach, while during a transition to $\Delta T_{2\times CO_2}$ both corrections for unconsidered slow feedbacks and the potential state-dependent character of $S_{[X]}$ need to be considered with care to avoid overestimations. However, we like to emphasize again (as done already in Snyder (2017)) that the approach to calculate $S_{[X]}$ based on paleodata defined in PALAEOSENS-Project Members (2012) and used in Snyder (2016) and here does not test causation. Those processes considered as "forcing," such as land ice albedo and CO_2 radiative forcing in $S_{[CO_2,LI]}$, are typically those for which paleodata exist, and not those which are believed to be responsible for the paleoclimate changes. Because causation was not suggested by the different setups, 10 different permutation of $S_{[X]}$ have been calculated in PALAEOSENS-Project Members (2012).

Especially due to the state-dependent character of $S_{[X]}$ necessary corrections for other slow feedbacks and a detailed calculation of S^a based on $S_{[CO_2,LI]}$ are not readily available for $\Delta R_{[CO_2,LI]} = 0$ W m^{-2}. Therefore, a detailed calculation of S^a is beyond the scope of this study. Nevertheless, this paleodata-based analysis suggests that the equilibrium climate sensitivity for present-day is more at the high end with respect to reported values in the IPCC AR5 report (e.g., Thematic Focus Element 6 in Stocker et al., 2013). Other paleostudies applying climate models of different complexity to various different climate background states, which have been up to 16 K warmer than the preindustrial climate, also found a state dependency in $S_{[CO_2,LI]}$ with mean numbers ranging from 0.6 to 1.6 K W^{-1} m^2 (von der Heydt et al., 2016).

References

Ahn, J., & Brook, E. J. (2014). Siple Dome ice reveals two modes of millennial CO_2 change during the last ice age. *Nature Communications*, *5*, 3723. https://doi.org/10.1038/ncomms4723

Armour, K. C., Bitz, C. M., & Roe, G. H. (2013). Time-varying climate sensitivity from regional feedbacks. *Journal of Climate*, *26*(13), 4518–4534. https://doi.org/10.1175/JCLI-D-12-00544.1

Bereiter, B., Eggleston, S., Schmitt, J., Nehrbass-Ahles, C., Stocker, T. F., Fischer, H., … Chappellaz, J. (2015). Revision of the EPICA Dome C CO_2 record from 800 to 600 kyr before present. *Geophysical Research Letters*, *42*, 542–549. https://doi.org/10.1002/2014GL061957

Bereiter, B., Lüthi, D., Siegrist, M., Schüpbach, S., Stocker, T. F., & Fischer, H. (2012). Mode change of millennial CO_2 variability during the last glacial cycle associated with a bipolar marine carbon seesaw. *Proceedings of the National Academy of Sciences*, *109*(25), 9755–9760. https://doi.org/10.1073/pnas.1204069109

Bloch-Johnson, J., Pierrehumbert, R. T., & Abbot, D. S. (2015). Feedback temperature dependence determines the risk of high warming. *Geophysical Research Letters*, *42*, 4973–4980. https://doi.org/10.1002/2015GL064240

Crucifix, M. (2006). Does the Last Glacial Maximum constrain climate sensitivity? *Geophysical Research Letters*, *33*, L18701. https://doi.org/10.1029/2006GL027137

de Boer, B., Lourens, L. J., & van de Wal, R. S. (2014). Persistent 400,000-year variability of Antarctic ice volume and the carbon cycle is revealed throughout the Plio-Pleistocene. *Nature Communications*, *5*, 2999. https://doi.org/10.1038/ncomms3999

de Boer, B., van de Wal, R. S., Lourens, L. J., & Bintanja, R. (2012). Transient nature of the Earth's climate and the implications for the interpretation of benthic records. *Palaeogeography, Palaeoclimatology, Palaeoecology*, *335–336*, 4–11. https://doi.org/10.1016/j.palaeo.2011.02.001

Friedrich, T., Timmermann, A., Tigchelaar, M., Elison Timm, O., & Ganopolski, A. (2016). Nonlinear climate sensitivity and its implications for future greenhouse warming. *Science Advances*, *2*(11), e1501923. https://doi.org/10.1126/sciadv.1501923

Gregory, J. M., Ingram, W. J., Palmer, M. A., Jones, G. S., Stott, P. A., Thorpe, R. B., … Williams, K. D. (2004). A new method for diagnosing radiative forcing and climate sensitivity. *Geophysical Research Letters*, *31*, L03205. https://doi.org/10.1029/2003GL018747

Hansen, J., Sato, M., Kharecha, P., & von Schuckmann, K. (2011). Earth's energy imbalance and implications. *Atmospheric Chemistry and Physics*, *11*(24), 13,421–13,449. https://doi.org/10.5194/acp-11-13421-2011

Hansen, J., Sato, M., Russell, G., & Kharecha, P. (2013). Climate sensitivity, sea level and atmospheric carbon dioxide. *Philosophical Transactions of the Royal Society A: Mathematical, Physical and Engineering Sciences*, *371*, 20120294. https://doi.org/10.1098/rsta.2012.0294

Hargreaves, J. C., Abe-Ouchi, A., & Annan, J. D. (2007). Linking glacial and future climates through an ensemble of GCM simulations. *Climate of the Past*, *3*, 77–87. https://doi.org/10.5194/cp-3-77-2007

Hasenclever, J., Knorr, G., Rüpke, L., Köhler, P., Morgan, J., Garofalo, K., . . . Hall, I. (2017). Sea level fall during glaciation stabilized atmospheric CO_2 by enhanced volcanic degassing. *Nature Communications*, 8, 15867. https://doi.org/10.1038/ncomms15867

Hönisch, B., Hemming, N. G., Archer, D., Siddall, M., & McManus, J. F. (2009). Atmospheric carbon dioxide concentration across the mid-Pleistocene transition. *Science*, 324(5934), 1551–1554. https://doi.org/10.1126/science.1171477

Jonko, A. K., Shell, K. M., Sanderson, B. M., & Danabasoglu, G. (2013). Climate feedbacks in CCSM3 under changing CO_2 forcing. Part II: Variation of climate feedbacks and sensitivity with forcing. *Journal of Climate*, 26(9), 2784–2795. https://doi.org/10.1175/JCLI-D-12-00479.1

Köhler, P., Bintanja, R., Fischer, H., Joos, F., Knutti, R., Lohmann, G., & Masson-Delmotte, V. (2010). What caused Earth's temperature variations during the last 800,000 years? Data-based evidences on radiative forcing and constraints on climate sensitivity. *Quaternary Science Reviews*, 29, 129–145. https://doi.org/10.1016/j.quascirev.2009.09.026

Köhler, P., de Boer, B., von der Heydt, A. S., Stap, L. S., & van de Wal, R. S. W. (2015). On the state dependency of equilibrium climate sensitivity during the last 5 million years. *Climate of the Past*, 11, 1801–1823. https://doi.org/10.5194/cp-11-1801-2015

Laskar, J., Robutel, P., Joutel, F., Gastineau, M., Correia, A. C. M., & Levrard, B. (2004). A long term numerical solution for the insolation quantities of the Earth. *Astronomy and Astrophysics*, 428, 261–285. https://doi.org/10.1051/0004-6361:20041335

Lisiecki, L. E., & Raymo, M. E. (2005). A Pliocene-Pleistocene stack of 57 globally distributed benthic δ^{18}O records. *Paleoceanography*, 20, PA1003. https://doi.org/10.1029/2004PA001071

Lunt, D. J., Haywood, A. M., Schmidt, G. A., Salzmann, U., Valdes, P. J., & Dowsett, H. J. (2010). Earth system sensitivity inferred from Pliocene modelling and data. *Nature Geoscience*, 3(1), 60–64. https://doi.org/10.1038/ngeo706

MacFarling-Meure, C., Etheridge, D., Trudinger, C., Langenfelds, R., van Ommen, T., Smith, A., & Elkins, J. (2006). Law Dome CO_2, CH_4 and N_2O ice core records extended to 2000 years BP. *Geophysical Research Letters*, 33, L14810. https://doi.org/10.1029/2006GL026152

Marcott, S. A., Bauska, T. K., Buizert, C., Steig, E. J., Rosen, J. L., Cuffey, K. M., . . . Brook, E. J. (2014). Centennial scale changes in the global carbon cycle during the last deglaciation. *Nature*, 514, 616–619. https://doi.org/10.1038/nature13799

Martínez-Botí, M. A., Foster, G. L., Chalk, T. B., Rohling, E. J., Sexton, P. F., & Lunt, D. J. (2015). Plio-Pleistocene climate sensitivity evaluated using high-resolution CO_2 records. *Nature*, 518, 49–54. https://doi.org/10.1038/nature14145

Meraner, K., Mauritsen, T., & Voigt, A. (2013). Robust increase in equilibrium climate sensitivity under global warming. *Geophysical Research Letters*, 40, 5944–5948. https://doi.org/10.1002/2013GL058118

Monnin, E., Indermühle, A., Dällenbach, A., Flückiger, J., Stauffer, B., Stocker, T. F., . . . Barnola, J.-M. (2001). Atmospheric CO_2 concentrations over the last glacial termination. *Science*, 291, 112–114. https://doi.org/10.1126/science.291.5501.112

Monnin, E., Steig, E. J., Siegenthaler, U., Kawamura, K., Schwander, J., Stauffer, B., . . . Fischer, H. (2004). Evidence for sustantial accumulation rate variability in Antarctica during the Holocene, through synchronization of CO_2 in the Taylor Dome, Dome C and DML ice cores. *Earth and Planetary Science Letters*, 224, 45–54. https://doi.org/10.1016/j.epsl.2004.05.007

Myhre, G., Highwood, E. J., Shine, K. P., & Stordal, F. (1998). New estimates of radiative forcing due to well mixed greenhouse gases. *Geophysical Research Letters*, 25, 2715–2718. https://doi.org/10.1029/98GL01908

PALAEOSENS-Project Members (2012). Making sense of palaeoclimate sensitivity. *Nature*, 491, 683–691. https://doi.org/10.1038/nature11574

Petit, J. R., Jouzel, J., Raynaud, D., Barkov, N. I., Barnola, J.-M., Basile, I., . . . Stievenard, M. (1999). Climate and atmospheric history of the past 420,000 years from the Vostok ice core, Antarctica. *Nature*, 399, 429–436. https://doi.org/10.1038/20859

Pierrehumbert, R., Abbot, D., Voigt, A., & Koll, D. (2011). Climate of the Neoproterozoic. *Annual Review of Earth and Planetary Sciences*, 39(1), 417–460. https://doi.org/10.1146/annurev-earth-040809-152447

Rohling, E. J., Marino, G., Foster, G. L., Goodwin, P., von der Heydt, A., & Köhler, P. (2018). Comparing climate sensitivity, past and present. *Annual Review of Marine Science*, 10. https://doi.org/10.1146/annurev-marine-121916-063242

Rohling, E. J., Medina-Elizalde, M., Shepherd, J. G., Siddall, M., & Stanford, J. D. (2012). Sea surface and high-latitude temperature sensitivity to radiative forcing of climate over several glacial cycles. *Journal of Climate*, 25, 1635–1656. https://doi.org/10.1175/2011JCLI4078.1

Rubino, M., Etheridge, D. M., Trudinger, C. M., Allison, C. E., Battle, M. O., Langenfelds, R. L., . . . Francey, R. J. (2013). A revised 1000-year atmospheric δ^{13}C-CO_2 record from Law Dome and South Pole, Antarctica. *Journal of Geophysical Research: Atmospheres*, 118, 8482–8499. https://doi.org/10.1002/jgrd.50668

Schmidt, G. A., Severinghaus, J., Abe-Ouchi, A., Alley, R. B., Broecker, W., Brook, E., . . . Stocker, T. F. (2017). Overestimate of committed warming. *Nature*, 547(7662), E16–E17. https://doi.org/10.1038/nature22803

Schneider, R., Schmitt, J., Köhler, P., Joos, F., & Fischer, H. (2013). A reconstruction of atmospheric carbon dioxide and its stable carbon isotopic composition from the penultimate glacial maximum to the last glacial inception. *Climate of the Past*, 9, 2507–2523. https://doi.org/10.5194/cp-9-2507-2013

Siegenthaler, U., Stocker, T. F., Monnin, E., Lüthi, D., Schwander, J., Stauffer, B., . . . Jouzel, J. (2005). Stable carbon cycle-climate relationship during the late Pleistocene. *Science*, 310, 1313–1317. https://doi.org/10.1126/science.1120130

Snyder, C. W. (2016). Evolution of global temperature over the past two million years. *Nature*, 538(7624), 226–228. https://doi.org/10.1038/nature19798

Snyder, C. W. (2017). Snyder replies. *Nature*, 547(7662), E17–E18. https://doi.org/10.1038/nature22804

Stocker, T., Qin, D., Plattner, G.-K., Alexander, L., Bindoff, S. A. N., Bréon, F.-M., . . . Xie, S.-P. (2013). Technical summary. In T. F. Stocker et al., (Eds.), *Climate change 2013: The physical science basis. Contribution of Working Group I to the Fifth Assessment Report of the Intergovernmental Panel on Climate Change* (pp. 33–116). Cambridge, UK: Cambridge University Press. https://doi.org/10.1017/CBO9781107415324.005

van de Wal, R. S. W., de Boer, B., Lourens, L., Köhler, P., & Bintanja, R. (2011). Reconstruction of a continuous high-resolution CO_2 record over the past 20 million years. *Climate of the Past*, 7(1), 1459–1469. https://doi.org/10.5194/cp-7-1459-2011

von der Heydt, A. S., & Ashwin, P. (2016). State dependence of climate sensitivity: attractor constraints and palaeoclimate regimes. *Dynamics and Statistics of the Climate System*, 1(1), dzx001. https://doi.org/10.1093/climsys/dzx001

von der Heydt, A. S., Dijkstra, H. A., W. van de Wal, R. S., Caballero, R., Crucifix, M., Foster, G. L., . . . Ziegler, M. (2016). Lessons on climate sensitivity from past climate changes. *Current Climate Change Reports*, 2, 148–158. https://doi.org/10.1007/s40641-016-0049-3

von der Heydt, A. S., Köhler, P., van de Wal, R. S., & Dijkstra, H. A. (2014). On the state dependency of fast feedback processes in (paleo) climate sensitivity. *Geophysical Research Letters*, 41, 6484–6492. https://doi.org/10.1002/2014GL061121

Yoshimori, M., Hargreaves, J. C., Annan, J. D., Yokohata, T., & Abe-Ouchi, A. (2011). Dependency of feedbacks on forcing and climate state in physics parameter ensembles. *Journal of Climate*, 24(24), 6440–6455. https://doi.org/10.1175/2011JCLI3954.1

Zeebe, R. E. (2013). Time-dependent climate sensitivity and the legacy of anthropogenic greenhouse gas emissions. *Proceedings of the National Academy of Sciences*, 110(34), 13,739–13,744. https://doi.org/10.1073/pnas.1222843110